Sensors & Diagnostics

PAPER

View Article Online
View Journal | View Issue

Cite this: *Sens. Diagn.*, 2024, **3**, 1513

Optimized gadolinium-DO3A loading in RAFT-polymerized copolymers for superior MR imaging of aging blood–brain barrier†

Hunter A. Miller,‡[a] Aaron Priester,‡[b] Evan T. Curtis,[a] Krista Hilmas,[c] Ashleigh Abbott,[d] Forrest M. Kievit [a] and Anthony J. Convertine *[b]

The development of gadolinium-based contrast agents (GBCAs) has been pivotal in advancing magnetic resonance imaging (MRI), offering enhanced soft tissue contrast without ionizing radiation exposure. Despite their widespread clinical use, the need for improved GBCAs has led to innovations in ligand chemistry and polymer science. We report a novel approach using methacrylate-functionalized DO3A ligands to synthesize a series of copolymers through direct reversible addition-fragmentation chain transfer (RAFT) polymerization. This technique enables precise control over the gadolinium content within the polymers, circumventing the need for subsequent conjugation and purification steps, and facilitates the addition of other components such as targeting ligands. The resulting copolymers were analysed for their relaxivity properties, indicating that specific gadolinium-DO3A loading contents between 12–30 mole percent yield optimal MRI contrast enhancement. Inductively coupled plasma (ICP) measurements corroborated these findings, revealing a non-linear relationship between gadolinium content and relaxivity. Optimized copolymers were synthesized with the claudin-1 targeting peptide, C1C2, to image BBB targeting in aged mice to show imaging utility. This study presents a promising pathway for the development of more efficient GBCA addition to copolymers for targeted drug delivery and bioimaging application.

Received 26th February 2024,
Accepted 14th July 2024

DOI: 10.1039/d4sd00063c

rsc.li/sensors

Introduction

Magnetic Resonance Imaging (MRI) has emerged as a critical tool in diagnostic medicine, offering high-resolution images of soft tissue without the risks associated with ionizing radiation. The contrast in MRI is primarily achieved through the relaxation of water protons, a process that can be enhanced by contrast agents (CAs). Among various elements used for this purpose, gadolinium (Gd^{3+}) stands out. It has 7 unpaired electrons which yield a high magnetic moment (7.94 μB),[1] and it has long electron spin relaxation times (10^{-9}–10^{-8} s).[1] These properties make it excellent at enhancing proton relaxation and the most widely used metal in T1 contrast agents for MRI. However, the inherent toxicity of free Gd^{3+} necessitates its use in a bound form to prevent *in vivo* metal ion release. This has led to the development of various gadolinium-based contrast agents (GBCAs). The first GBCA, Gd-DTPA, was approved in 1988, marking a significant milestone in clinical MRI applications. Subsequent developments in the 1990s led to the creation of various extracellular space-targeting GBCAs. Further advancements saw the introduction of liver-targeting GBCAs, such as Gd-BOPTA in Europe and Gd-EOB-DTPA, signifying the evolution and diversification of GBCAs for specific organ imaging. Gd-labeled polymeric nanoparticles have previously been synthesized by complexation of Gd^{3+} to carboxylates within the polymer chain, encapsulating then within the core or attaching them *via* surface functionalization. Gd-labeled linear polymeric macromolecules such as poly(lysines) or poly(amino acids) have also gained attraction due to their high Gd loading capacity or large number of residues accessible for conjugation. R1 relaxivity values for Gd-containing nanomaterials in these studies have ranged anywhere from 3.05–10.8 mM^{-1} s^{-1}, providing excellent MRI contrast.[2–5] Despite their widespread clinical use over the past

[a] *Department of Biological Systems Engineering, University of Nebraska-Lincoln, 262 Morrison Center, Lincoln, NE 68583, USA*
[b] *Department of Materials Science and Engineering, Missouri University of Science and Technology, 1400 North Bishop Avenue, Rolla, MO 65409, USA. E-mail: convertinea@mst.edu*
[c] *Joint Department of Biomedical Engineering, North Carolina State University and The University of North Carolina at Chapel Hill, Raleigh, NC, 27695, USA*
[d] *J. Crayton Pruitt Family Department of Biomedical Engineering, University of Florida- Gainesville, 1275 Center Drive, Gainesville, FL, 32611, USA*
† Electronic supplementary information (ESI) available. See DOI: https://doi.org/10.1039/d4sd00063c
‡ Equally contributing co-first authors.

28 years in over 300 million patients, GBCAs continue to evolve, driven by advances in MRI technology and the development of new agents.

The evolution of GBCAs has been significantly influenced by the selection of appropriate ligands and the development of various conjugation chemistries. The choice of ligand plays a pivotal role in the stability, toxicity, and efficacy of GBCAs. Among the chelating ligands used, DOTA (1,4,7,10-tetraazacyclododecane-1,4,7,10-tetraacetic acid) has gained prominence due to its high thermodynamic stability and kinetic inertness, which are crucial in preventing the release of toxic Gd^{3+} ions *in vivo*. DOTA and its derivatives have become an essential part of improving clinical safety related to limiting both nephrogenic systemic fibrosis (NSF) and Gd deposition.[6] In addition to chelating ligand selection, various conjugation chemistries have been employed to durably incorporate Gd into different molecular frameworks. The thoughtful design of such molecules can expand the capabilities of GBCAs by altering *in vivo* behavior and contrast enhancement. Regarding biodistribution, amide and ester linkages are commonly used for conjugating Gd chelates to targeting vectors or biomolecules. Targeted nanomaterial GBCAs have previously been implemented in preclinical imaging of various cancers.[7] The further refinement of GBCAs will expedite the investigation of novel targeting strategies and the resulting expansion of MRI-based diagnostic capabilities. In this work, the developed GBCA is joined with C1C2, a peptide targeting claudin-1, to investigate *in vivo* targeting efficacy. Claudin-1 is a tight junction protein that appears to be ectopically overexpressed in brain vasculature in stroke and during aging.[8,9] The use of GBCAs with targeting moieties enables use of dynamic contrast-enhanced (DCE-) MRI, which has been used clinically to assess blood–brain barrier (BBB) permeation in pathologic conditions such as traumatic brain injury, stroke, and aging.[10–15]

The design of the GBCA molecular framework also affects contrast enhancement through various mechanisms. Attaching Gd to larger structures can benefit contrast by slowing molecular tumbling rates, thereby decreasing diffusional and rotational correlation times.[16,17] Another factor in contrast performance is the association of Gd with water. The degree to which Gd increases contrast is related to the number of water molecules that can simultaneously associate with Gd, called the hydration state q. The more water molecules that can associate with Gd, the more rapidly Gd can enhance the relaxation of the bulk water. In addition, the rate of exchange of bound water affects contrast enhancing properties. Furthermore, the distance (d) between the Gd and water molecules is inversely correlated with contrast enhancing properties as the strength of the dipolar mechanism decays with $1/d$.[6] Previous work has shown that the Gd loading rate in nanomaterials can influence these Gd–water interactions, altering the T1 contrast enhancement.[17,18] The morphology of the molecular framework influences contrast *via* the interaction of these factors.

Recently we reported the development of a polymerizable DOTA ligand, which was utilized to construct theranostic neuroprotective copolymers integrated with gadolinium-based MRI contrast agents.[19] This advancement underscores the potential of polymerizable DOTA ligands in the incorporation of gadolinium ligands into polymers. Employing controlled Reversible Addition-Fragmentation Chain Transfer (RAFT) polymerization, this method provides a more streamlined and potentially cost-effective approach for producing GBCAs. In the current context, we shift our focus towards further exploring polymerizable DOTA ligands, specifically aiming to determine the optimal gadolinium DOTA concentration in various copolymers. This investigation is directed towards enhancing both the efficiency and safety of GBCAs, thereby contributing to the advancement of MRI diagnostics. The developed GBCA was then tested *in vivo* with a targeting ligand, C1C2, to illustrate one application of this novel macromolecular system.

Experimental procedures

Materials

The following chemicals were obtained from Chem Impex Int'l: 4-dimethylaminopyridine (DMAP, 99.43%), 3-(3-dimethylaminopropyl)-1-ethyl-carboiimide hydrochloride (EDC, 99.9%), 1,3-dicyclohexylcarbodiimide (DCC, 99.42%), bromoacetic acid *tert*-butyl ester (99.35%), cyclen (99.6%), dichloromethane (99.91%), *N*,*N*-dimethylacetamide anhydrous (DMAc, 99.93%), dimethylformamide (DMF, 99.98%) and trifluoroacetic acid (TFA, 99.9%). O950 (poly(ethylene glycol) methyl ether methacrylate), gadolinium(III) chloride hexahydrate (99.9%), mono-2-(methacryloyloxy)ethyl succinate (SMA), sodium acetate trihydrate (>99.5%), 4,4′ azobis (4-cyanovaleric acid) (ABCVA, >98%), hydroxyethyl methacrylate (HEMA) and deuterium oxide (D_2O 99.8 at%) were obtained from Sigma Aldrich. Chloroform-*d* ($CDCl_3$, 99.8% w/ 1% TMS) was obtained from Thermo Scientific. Hexanes (mixed isomers, 98+%) and methanol (>99%) were obtained from Alfa Aesar. 4-((((2-Carboxyethyl)thio)carbonothioyl)thio)-4-cyanopentanoic acid (CCC, 95%) was obtained from Boron Molecular. Oxalyl chloride (>98%) and triethylamine (TEA, >99%) were obtained from TCI. Potassium hydroxide (KOH) was obtained from Fisher Scientific.

Synthesis of di-*tert*-butyl 2,2′-(4-(2-isopropoxy-2-oxoethyl)-1,4,7,10-tetraazacyclododecane-1,7-diyl)diacetate (BOC DO3A). Precursor material BOC DO3A (1,4,7,10-tetraazacyclododecane-1,4,7-triacetic acid, tri-*tert*-butyl ester hydrobromide) for BOC DO3A-MA was synthesized as described previously.[20] Briefly, to a 1 L round bottom flask was added cyclen (25 g, 0.145 moles), sodium acetate trihydrate (65 g, 0.478 moles), and 200 mL of dimethylacetamide and stirred for 30 minutes. A solution of bromoacetic acid *tert*-butyl ester (93.5 g, 0.478 moles) and

dimethylacetamide (200 mL) was then added dropwise over 90 minutes or added dropwise while the temperature was kept between 25–30 °C. The stirred solution was then allowed to react for ~60 hours. To the gelatinous white solution was then added 100 mL of diethyl ether after which the mixture was placed in the freezer at −20 °C for three hours. After this time, the mixture was vacuum filtered, washed once with cold dimethylacetamide (50 mL × 2) followed by cold diethyl ether (125 mL × 2). The crude powder was then dissolved into 500 mL and then transferred to a separation funnel where it was washed three times with distilled water and twice with saturated brine solution. The organic phase was then dried over $MgSO_4$ and rotary evaporated until a thin oil of ~200 g remained. The oil was diluted with 400 mL of hexanes and allowed to stir until the product re-crystallized. The resultant product was then washed with cold hexanes and then dried under vacuum yielding 50 g of a white solid (58% yield). ^{1}H NMR in $CDCl_3$ of BOC DO3A precursor powder is shown in ESI† Fig. S1A. All NMR measurements were made on the Nanalysis 60 MHz benchtop ^{1}H NMR.

Synthesis of 2-(methacryloyloxy)ethyl 4-chloro-4-oxobutanoate (SMA Cl). To a 250 mL flat bottomed flask was added dichloromethane (73 mL) and dimethylformamide (730 μL). The solution was then cooled to −20 °C after which time the round bottom flask was transferred to an ice bath. To this solution oxalyl chloride (20 g, 0.157 moles) was then added dropwise with stirring over 10 minutes. A solution of SMA (18.1 g, 0.08 moles) in dichloromethane (18.1 g) was then added dropwise added to the oxalyl chloride solution. The solution was then allowed to react for two hours after which time the acid chloride was isolated by rotary evaporation and used without further purification. ^{1}H NMR of isolated SMA Cl in $CDCl_3$ is shown in ESI† Fig. S1B.

Synthesis of tri-*tert*-butyl 2,2′,2″-(10-(4-(2-(methacryloyloxy) ethoxy)-4-oxobutanoyl)-1,4,7,10-tetraazacyclododecane-1,4,7-triyl)triacetate (BOC DO3A-MA). To a 250 mL round bottom flask was added TRI-BOC (10 g) and 250 mL of dichloromethane. The solution was then transferred to an ice bath and a solution of triethylamine (3.78 g, 0.037 moles) and dichloromethane (10 mL) was added dropwise. The solution was then cooled to −20 °C in the freezer. To the chilled solution, SMA acid chloride (4.65 g) in dichloromethane (25 mL) was then added dropwise over 20 minutes after which time the reaction was allowed to proceed for 20 hours. After this time, the solution was transferred to a separation funnel where it was washed once with distilled water and then three times with sodium bicarbonate (0.6 M). The organic phase was then dried over $MgSO_4$ and then rotary evaporated to yield the product (11.9 g, −81% yield). ^{1}H NMR of BOC DO3A-MA monomer in $CDCl_3$ is shown in ESI† Fig. S1C.

Deprotection of BOC DO3A-MA (DO3A-MA synthesis). (1 g) was mixed with 6 mL of a 75% by volume solution of TFA in methylene chloride. The solution was then stirred for 18 hours after which time the methylene chloride and TFA were removed by rotary evaporation. ^{1}H NMR of deprotected BOC DO3A-MA (simply, DO3A-MA) in D_2O is shown in ESI† Fig. S1D.

Synthesis of poly((DO3A-MA)-co-0950) series (MRI series copolymers) and C1C2 peptide-targeted 12 wt% DO3A-MA copolymer. Copolymerizations of DO3A-MA and O950 were conducted in DMAc at an initial total comonomer concentration of 50 wt% with a CTA to initiator ratio ($[CTA]_0/[I]_0$) of 10 to 1 and a monomer to CTA ratio ($[M]_0/[CTA]_0$) of 25 to 1. The weight ratios of BOC DO3A-MA to O950 were varied to yield a series of polymerizations with between 4 and 40 wt% DOTA. Polymerization solutions were purged with argon for 30 minutes and then transferred to a preheated water bath at 70 °C for 24 hours. Following polymerization, the copolymer solutions were transferred to Spectrapor regenerated cellulose dialysis membranes (preequilibrated in distilled water) and then dialyzed against acetone (×2) for one day followed by deionized water (×3) for two additional days. Following dialysis, the polymerization solutions were frozen and then isolated by lyophilization. A representative procedure for the 12 wt% DO3A-MA copolymer is as follows: to a 5 mL round bottom flask was added O950 (0.88 g, 0.926 mmol), DO3A-MA (0.12 g, 0.215 mmol), 0.27 g of a 50 mg g^{-1} CCC stock in DMAc (13.5 mg, 44.9 μmol), 0.24 g of a 5 mg g^{-1} ABCVA in DMAc (1.20 mg, 4.28 μmol), DMAc (0.43 g) and 84 μL of 59.5 mg mL^{-1} REMA stock in DMF. Quantitative monomer conversion was confirmed by ^{1}H NMR in $CDCl_3$ by following the disappearance of the vinyl resonances (2H, 5.5 and 6.0 ppm) of the monomers relative to a DMF reference peak (1H, 8 ppm). ^{1}H NMR of purified polymers in D_2O were measured prior to complexation. After Gd^{3+} optimization experiments, the polymerization conditions above for the 12 wt% DO3A-MA were repeated but now included a DP 1 C1C2 peptide targeting monomer (0.135 g, 43.9 μmoles). Additionally, this new polymerization was conducted in DMSO as opposed to DMAc as the peptide monomer was insoluble in DMAc. All other conditions were kept the same. Mass spectroscopy for the synthesized C1C2 monomer can be found in ESI† Fig. S2 and S3.

GPC analysis of poly((DO3A-MA)-co-O950) series polymers. In preparation for GPC measurements, 0.4 g of each poly((DO3A-MA)-co-O950) series polymer were esterified with methanol (1.5 mL, 36.9 mmoles) using 4-dimethylaminopyridine (DMAP, 0.10 g, 0.819 mmoles) as catalyst and 3-(3-dimethylaminopropyl)-1-ethyl-carbodiimide (EDC, 0.16 g, 0.835 mmoles) as coupling agent. Molecular weights for the copolymer series were determined using the Agilent Gel Permeation Chromatographer (GPC) with PMMA standards and DMF + 1% LiBr as the solvent.

Gd complexation of poly((DO3A-MA)-co-O950) series polymers. A stock solution of $GdCl_3{\cdot}6H_2O$ in distilled water (200 mg mL^{-1}) was made in preparation for complexation. $GdCl_3{\cdot}6H_2O$ was added to each polymer solution in a 3× molar excess with respect to DO3A-MA residues. A series of dilutions of $GdCl_3{\cdot}6H_2O$ solution were prepared such that 1 mL of each concentration could be added to each series copolymer. Copolymers were dissolved in 14 mL of distilled

water followed by addition of 1 mL of the appropriate Gd stock concentration. pH of the solution was adjusted to 6 using 1 M KOH solution in distilled water. Polymer solutions with Gd were then placed in 25 mL round bottom flasks, sealed with rubber septa and parafilm and placed in a pre-heated water bath overnight at 40 °C (~18 h). Polymer solutions were then transferred into regenerated cellulose dialysis tubing (12–14 kDa cutoff) and dialyzed against distilled water for 3 days. Purified polymer solutions were frozen and lyophilized. Following lyophilization, C1C2-containing polymer was dispersed in buffer at a concentration of 10 mg mL^{-1} and run through a PD10 desalting column. The eluent was collected, frozen and lyophilized.

Relaxivity characterization. T1 and T2 relaxivity of samples were measured using a 9.4 T MRI (Varian) equipped with a 4 cm Millipede RF imaging probe with triple-axis gradients (100 G cm^{-1} max). Solutions of GPDNs across the range of wt% DO3A-MA residues were prepared at 7 Gd(III) concentrations from 0.25–0 mM diluted in PBS. Prepared samples were arranged in a custom sample holder and imaged first using a fast spin-echo sequence for T1 mapping, then with a multi-echo multi-slice sequence for T2 mapping. The parameters common for both sequences were as follows: temperature = 22 °C, field of view (FOV) = 25 × 25 × 3 mm^3, matrix size = 128 × 128 voxels. The fast spin-echo sequence had the following additional parameters: 11 repetition times (TRs) logarithmically spaced from 200–12 000 ms, effective echo time (TE) = 20.67 ms, echo train length = 8, echo spacing = 5.17 ms, number of averages = 2. MATLAB was used to map T1 by fitting signal to the following equation:

$$S = S_0\left(1 - e^{\frac{-TR}{T1}}\right)$$

where S is the measured signal in a voxel, S_0 is the signal in that voxel at saturation, TR is the repetition time, and T1 is the longitudinal relaxation time.

The multi-echo sequence had the following additional parameters: TR = 3000 ms, number of echoes = 10, 10 TEs linearly spaced from 10–100. T2 mapping was also performed in MATLAB using the following equation:

$$S = A \cdot e^{-\frac{TE}{T2}}$$

where S is the measured signal in a voxel, A is a scaling factor, TE is the echo time, and T2 is the transverse relaxation time. From the T1 and T2 maps, r1 and r2 were then calculated as the slope of the plots of 1/T1 or 1/T2 *versus* Gd concentration.

In vivo DCE-MRI of targeted and non-targeted polymers

DCE-MRI was performed using the same 9.4 T MRI system (Varian) above to assess the effect of targeting agent C1C2 on tissue accumulation as previously described.[8,13] Briefly, CD-1 mice (Charles River) were induced and maintained with 1–2% isoflurane to maintain 50–80 breaths per minute. Pre-contrast gradient-echo images were collected at two flip angles (FAs), 10^0 and 30^0, for T1 mapping with the variable flip angle method.[21,22] Mice were injected *via* tail-vein catheter with 100 μL 12% poly((DO3A-MA)-co-O950) copolymers with or without C1C2 along with 100 μL PBS. The injection was followed by 45 minutes of post-contrast imaging. All post-contrast gradient-echo scans used the following parameters: TR = 54.28 ms, TE = 2.73 ms, FA = 30^0, FOV = 20 × 20 × 10 mm^3, 10 slices of 1 mm thickness, matrix size = 128 × 128 voxels, number of averages = 4. Following image acquisition, R1, concentration, and K^{trans} maps were generated using a custom MATLAB script. R1 maps used the variable flip angle method with the following equation:[21]

$$\frac{S_{SPGR}}{\sin(\alpha)} = \frac{S_{SPGR}}{\tan(\alpha)} \cdot e^{\frac{TR}{T1}} + M_0\left(1 - e^{\frac{TR}{T1}}\right)$$

where S_{SPGR} is signal intensity, α is FA, and M_0 is a proportionality factor related to the longitudinal magnetization. Concentration maps were then made by comparing baseline R1 and post-contrast R1 maps with the following equation:

$$C(t) = \frac{R1(t) - R1(t_0)}{r1}$$

where $C(t)$ is the concentration at time t, $R1(t)$ is the post contrast R1 at t, $R1(t_0)$ is the baseline R1, and r1 is the relaxivity of the contrast agent. K^{trans}, the contrast extravasation rate constant, was then calculated based on the Patlak model and the following equation:

$$C(t) = v_p C_a(t) + K^{trans} \otimes C_a(t)$$

where C is the tissue concentration, C_a is the arterial plasma concentration, v_p is the plasma volume fraction, and ⊗ is convolution. The use of the Patlak model is supported by previous work in assessment of the subtle BBB permeability changes related to aging.[8,23,24] Statistical analysis comparing mean values of K^{trans} was completed using a t-test with Bonferroni correction. Significance was set as corrected p values less than 0.05.

Results and discussion

The direct controlled polymerization process employed for integrating chelating ligands into therapeutic polymers effectively eliminates the need for additional conjugation and purification steps. Utilizing a methacrylate-functionalized DO3A ligand (DO3A-MA), the procedure begins with the selective protection of three out of the four amine groups on the cyclen molecule with BOC groups, as described by Moore *et al.*[20] This leaves one amine group free to react with SMA Cl, subsequently introducing a single methacrylate group for polymerization. The final step in the synthesis involves the deprotection of the BOC groups under strongly acidic

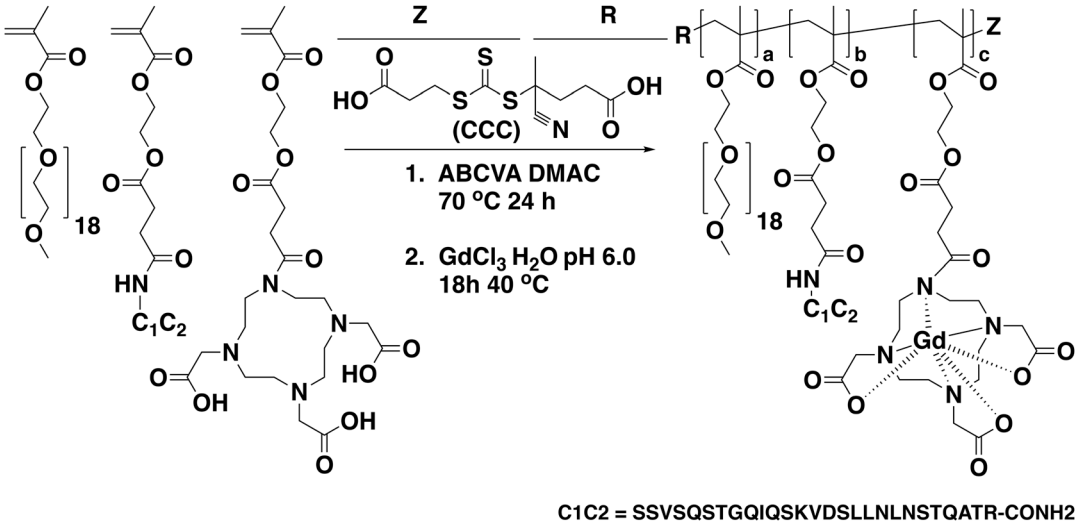

Scheme 1 Synthetic scheme for the preparation of gadolinium-functional polymers *via* the direct RAFT copolymerization of O950 and DO3A-MA along with the addition of a peptide-targeting monomer (C1C2).

conditions, revealing the active amine sites essential for the gadolinium chelating functionality of the monomer.

The synthetic process employed to synthesize copolymers of poly(ethylene glycol) methyl ether methacrylate (O950) DO3A-MA is shown in Scheme 1. Here copolymerization was conducted in DMAc with at a total monomer concentration of 50 wt%. These polymerizations employed a trithiocarbonate-based RAFT agent (CCC), with a CTA to initiator ratio ($[CTA]_0/[I]_0$) of 10 : 1 and a monomer to CTA ratio ($[M]_0/[CTA]_0$) of 25 : 1. Adjustments to the molar ratios of Gd-MA to O950 yielded copolymers with varying DOTA residues, from 4 to 50 wt%. The polymerization solutions were purged with argon for 30 minutes before being heated to 70 °C for a 24-hour reaction period. Following purification, the copolymer compositions were determined by ^{1}H NMR spectroscopy. A representative ^{1}H NMR spectra for the copolymer series is shown for the 12 wt% DO3A-MA copolymer in ESI† Fig. S4. Copolymer molar masses and molar mass dispersity values were determined *via* GPC in DMF + 1% LiBr. These results are shown graphically in a waterfall plot in ESI† Fig. S5. The shift in the retention time for the different copolymers is very subtle due to the log scale of molecular weight and the target molecular weight and conversion for the entire copolymer series. As shown by GPC, all traces were unimodal and narrow, indicating sufficient control over the RAFT polymerizations. Gadolinium was then introduced to the copolymers by incubating them with gadolinium chloride in water at pH 6.0 for 18 hours.

Gadolinium concentrations within the copolymer series were determined using Inductively Coupled Plasma Mass Spectrometry (ICP-MS) measurements, with the results presented in Table 1. Concentrations ranged from 0.496 mM for the 4% Gd-DO3A-MA copolymer to 28.175 mM for the 40% Gd-DO3A-MA copolymer, allowing for a correlation between the gadolinium content and relaxivity properties to be established. The ICP data indicated a non-linear correlation between the Gd-DO3A-MA percentage in the copolymers and the resulting gadolinium concentration in the solutions. Particularly, the 40% and 50% Gd-DO3A-MA copolymers showed significant increases in gadolinium concentration. This association underscores the influence of gadolinium concentration on the magnetic behaviour of the copolymers, a factor critical to their application as MRI contrast agents.

MRI was used to measure R1 relaxivity (r1) and R2 relaxivity (r2) of the copolymer series at 9.4 T. Such a measurement is essential for assessing their utility as MRI contrast agents. r1 exhibited a peak at the 12% Gd-DOTA concentration, with a value of 4.35 mM^{-1} s^{-1}, denoting a marked contrast enhancement. However, beyond this

Table 1 Polymer composition data, gadolinium quantification and relaxivity measurements

Sample	DO3A-MA feed (mol%)	DO3A-MA exp (mol%)	Mn, theo (kDa)	Mn, exp (kDa)	Monomer conversion (%)	Dispersity ($Đ$)	[Gd] (mM)	r1	r2	r2/r1
1	4	2	20.7	20.0	90	1.24	0.496	1.67	27.47	16.41
2	8	7	21.9	17.6	98	1.18	0.494	3.75	14.36	3.82
3	12	13	19.8	16.5	93	1.20	0.244	4.35	10.05	2.31
4	20	17	18.9	17.7	91	1.18	0.537	2.68	8.09	3.02
5	30	30	17.8	15.2	92	1.17	0.781	2.69	6.12	2.27
6	40	35	16.9	13.7	91	1.20	28.175	1.77	17.88	10.11
7	50	40	16.1	13.1	92	1.26	17.572	3.30	38.11	11.56

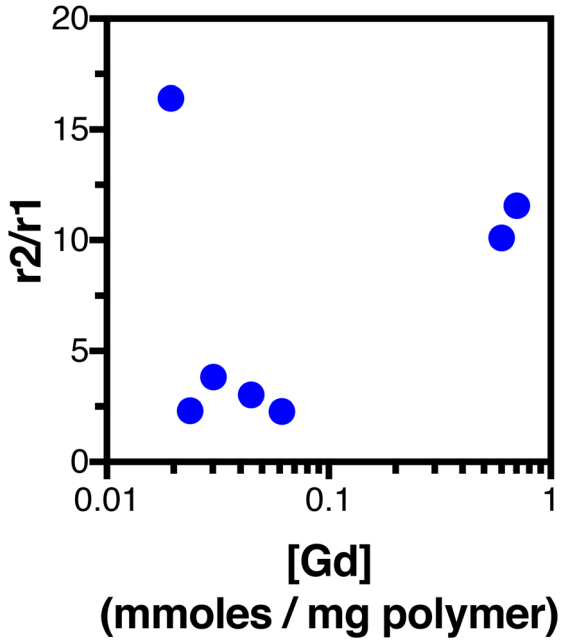

Fig. 1 r2/r1 ratio as a function of Gd concentration in (DO3A-MA)-co-O950 series polymers.

concentration, a decline in r1 was noted. This r1 value is lower than many reported in the literature for polymeric Gd-chelators. One polymer system incorporating Gd-AAZTA showed r1 of 16.4 mM^{-1} s^{-1} at 0.5 T,[25] while another based on Gd-DO3A showed r1 of 14.5 mM^{-1} s^{-1} at 0.47 T.[26] These r1 values are much higher, but the influence of field strength is relevant for proper interpretation. The copolymers presented here have molecular weights much higher than small molecule contrast agents, yielding longer rotational correlation times. At low field, this can greatly enhance r1, as seen in the examples referenced above. At higher field strengths however, the benefits to r1 decrease and all things equal a faster tumbling molecule may be preferred.[27] An additional factor affecting r1 is the water coordination time (τ_M) of the agent. τ_M is not quantified here, but previous studies of Gd-DO3A have shown relatively high values around 450–500 ns,[28,29] though the molecular context surrounding the chelator would impact the observed value. Considering r2, values decreased until the 30% concentration, beyond which an increase was observed, suggesting diminishing benefits at higher gadolinium levels. Correlating ICP-MS-measured gadolinium concentrations with MRI-derived relaxivity values provided insight into the observed trends. This was illustrated in Fig. 1, which showed the relationship between relaxivity ratio (r2/r1) and gadolinium-loading within the copolymer (mmoles Gd/mg polymer). The trend was somewhat U-shaped, showing high r2/r1 at either extreme of Gd-loading per mg polymer. The findings suggest a saturation effect in r1 at lower Gd levels and indicate a potential threshold beyond which transverse relaxation (R2) effects dominate with additional gadolinium, inhibiting positive contrast enhancement. The r2/r1 value of a contrast agent tends to increase with field strength, which can preclude its use for T1 contrast. The GBCA MS-325 which binds with human serum albumin has r2/r1 values at 1.4 T and 9.4 T of 2.4 and 14.7 mM^{-1} s^{-1}, respectively.[27] Further, Gadomer, a dendrimer-based GBCA shows r2/r1 values at 0.47 T and 4.7 T of 1.03 and 2.42 mM^{-1} s^{-1}, respectively.[30] Unfortunately, characterization of r2 is not ubiquitous in studies of GBCAs. Relaxivity values varied across Gd-MA feed percentages despite the proportional change in water coordinating ability. This may reflect limitation of water access to the inner-sphere of Gd^{3+} related to secondary structure or slow water exchange. Further investigation into the exact mechanisms of this difference is an interesting subject for future work. The observed r2/r1 ratio trends

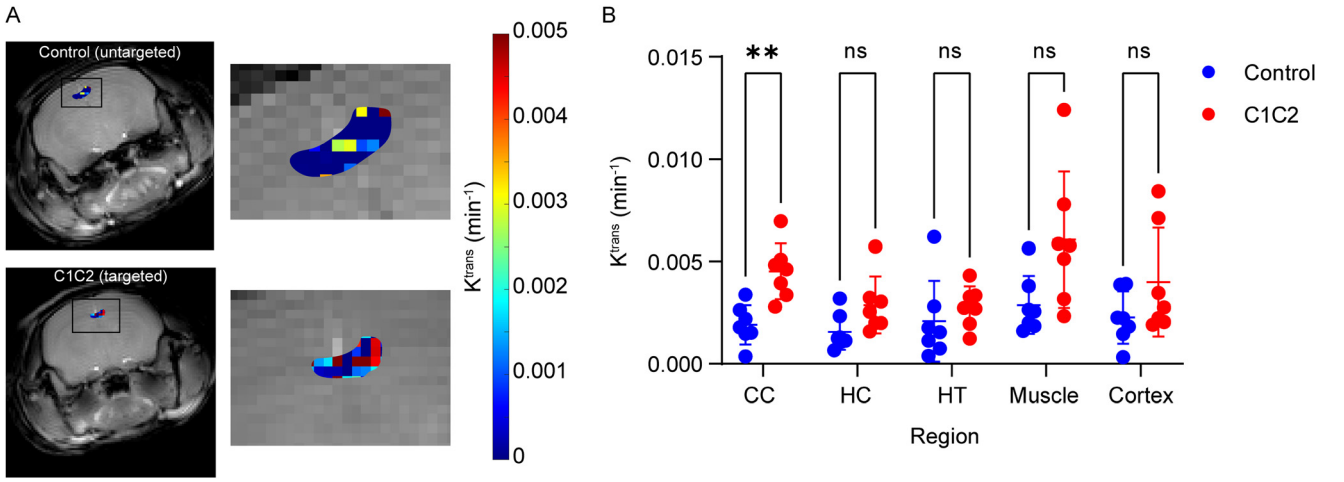

Fig. 2 Imaging C1C1 targeted and control GBCA copolymer accumulation in brain following intravenous administration in aged mice. (A) K^{trans} maps showing comparative accumulation in the corpus callosum (CC). (B) Comparison of accumulation determined by K^{trans} measurements in the CC, hippocampus (HC), hypothalamus (HT), muscle as a control, and cortex in aged mice. Statistical significance was determined by *t*-test with a Bonferroni correction.

confirmed the superior performance of the 8% and 12% Gd-DOTA concentrations in T1-weighted imaging. This ratio, alongside the relaxivity trends, implies a balance is achieved at these concentrations, effectively enhancing MRI contrast while considering the economic and safety implications of gadolinium usage. The 12% Gd-DO3A-MA level thus present the most promising characteristics for clinical MRI diagnostics. Continued research into the mechanisms behind these relaxivity properties is crucial and could inform the development of more refined GBCAs.

Following optimization of Gd-DO3A-MA levels at 12%, C1C2, a ligand targeting claudin-1, was introduced into the copolymers and tested in an *in vivo* model of normal aging. Previous work with C1C2-targeting has shown increases in both claudin-1 expression on the BBB and brain uptake, as measured with DCE-MRI, in aging mice. K^{trans} maps, showing the contrast extravasation rate constant at each voxel, were generated and regions of interest drawn in the corpus callosum (CC), the hippocampus (HC), the hypothalamus (HT), the cortex, and muscle. C1C2-targeting significantly increased copolymer uptake in the CC compared with the non-targeting control (Fig. 2). None of the other brain regions nor muscle showed significant differences between C1C2 and control copolymers. The increase in the CC was expected based on a similar finding in our previous work with C1C2-targeted Gd_2O_3 nanoparticles.[8] The present results diverge from the previous however in the HT and cortex, where no significant difference was shown here compared with drastic differences prior. While an effect of C1C2-targeting may have been expected in the HT and cortex, there are a number of differences between the two nanoparticle systems that may contribute to the observation. One major difference is in the orientation of the C1C2 peptide, which is inverted here relative to the previous work. This difference likely alters the interaction between C1C2 and claudin-1 on the endothelium, changing the rate of permeation from plasma into the brain parenchyma. Along with the C1C2 orientation, there are differences in the peptide loading density, which alters avidity and cellular internalization behavior.[31–33] Some additional factors lie with the mice: age, strain, and biological sex. The animals in this work were 13-month-old female CD-1 mice, while the previous work involved 12-month-old males and females from a C57BL/6J line. Differences between male and female mice in BBB permeability following traumatic brain injury have been seen by several groups including our own.[13,34,35] Despite these differences, the use of C1C2-targeting is shown as effective using the developed GBCA, illustrating its utility in future nanoparticle targeting and MRI diagnostic applications.

Conclusion

In conclusion, the direct RAFT copolymerization of polyethylene glycol methacrylate (O950) with a DO3A-MA has been demonstrated as an effective strategy for the synthesis of Gd-functional polymers. The optimized polymerization conditions, including the controlled monomer to CTA and CTA to initiator ratios, have resulted in copolymers with variable gadolinium content, exhibiting desirable relaxivity profiles suitable for MRI contrast applications. The ICP and relaxivity data suggest that certain gadolinium-DOTA concentrations within these copolymers offer improved contrast enhancement, with 8% and 12% concentrations providing the most promising results. This streamlined approach allowed for simple, one-pot synthesis of C1C2 peptide modified polymers for BBB targeting in aged mice. These findings reveal a facile synthesis approach for optimal MRI contrast enhancing properties of GBCA-modified copolymers and nanoparticles.

Data availability

The data supporting the results of this study have been included as part of the ESI.† Additionally, any datasets generated and analyzed during the current study are available from the corresponding author on reasonable request.

Conflicts of interest

There are no conflicts of interest to declare in this publication.

Acknowledgements

We acknowledge grant funding from the National Institute of Neurological Disorders and Stroke of the National Institutes of Health (R01NS109488) to FK and AC. This investigation is solely the responsibility of the authors and does not necessarily represent the official views of NINDS and NIH. All animal procedures were performed in accordance with approval by the University of Nebraska-Lincoln IACUC (protocol number 2300), which follows the Guide for the Care and Use of Laboratory Animals in the approval and monitoring of animal research protocols, and is accredited by the Association for Assessment and Accreditation of Laboratory Animal Care (AAALAC), USDA registered, and PHS assured.

References

1 L. Faucher, M. Tremblay, J. Lagueux, Y. Gossuin and M. A. Fortin, Rapid synthesis of PEGylated ultrasmall gadolinium oxide nanoparticles for cell labeling and tracking with MRI, *ACS Appl. Mater. Interfaces*, 2012, **4**(9), 4506–4515.
2 C. H. Reynolds, N. Annan, K. Beshah, J. H. Huber, S. H. Shaber, R. E. Lenkinski and J. A. Wortman, Gadolinium-Loaded Nanoparticles: New Contrast Agents for Magnetic Resonance Imaging, *J. Am. Chem. Soc.*, 2000, **122**, 8940–8945.
3 S. Suarez-Garcia, N. Arias-Ramos, C. Frias, A. P. Candiota, C. Arus, J. Lorenzo, D. Ruiz-Molina and F. Novio, Dual T1/T2 Nanoscale Coordination Polymers as Novel Constrast Agents for MRI: A Preclinical Stuy for Brain Tumor, *ACS Appl. Mater. Interfaces*, 2018, **10**(45), 38819–38832.

4 C. Huang and A. Tsourkas, Gd-based macromolecules and nanoparticles as magnetic resonance contrast agents for molecular imaging, *Curr. Top. Med. Chem.*, 2013, **13**(4), 411–421.
5 L. Esser, N. P. Truong, B. Karagoz, B. A. Moffat, C. Boyer, J. F. Quinn, M. R. Whittaker and T. P. Davis, Gadolinium-functionalized nanoparticles for application as magnetic resonance imaging contrast agents via polymerization-induced self-assembly, *Polym. Chem.*, 2016, **7**, 7325–7337.
6 M. Mathur, J. R. Jones and J. C. Weinreb, Gadolinium Deposition and Nephrogenic Systemic Fibrosis: A Radiologist's Primer, *Radiographics*, 2020, **40**(1), 153–162.
7 Z. Zhou and Z. R. Lu, Gadolinium-based contrast agents for magnetic resonance cancer imaging, *Wiley Interdiscip. Rev.: Nanomed. Nanobiotechnol.*, 2013, **5**(1), 1–18.
8 B. A. Bony, A. W. Tarudji, H. A. Miller, S. Gowrikumar, S. Roy, E. T. Curtis, C. C. Gee, A. Vecchio, P. Dhawan and F. M. Kievit, Claudin-1-Targeted Nanoparticles for Delivery to Aging-Induced Alterations in the Blood-Brain Barrier, *ACS Nano*, 2021, **15**(11), 18520–18531.
9 N. Sladojevic, S. M. Stamatovic, A. M. Johnson, J. Choi, A. Hu, S. Dithmer, I. E. Blasig, R. F. Keep and A. V. Andjelkovic, Claudin-1-Dependent Destabilization of the Blood–Brain Barrier in Chronic Stroke, *J. Neurosci.*, 2019, **39**(4), 743–757.
10 Z. Merali, K. Huang, D. Mikulis, F. Silver and A. Kassner, Evolution of blood-brain-barrier permeability after acute ischemic stroke, *PLoS One*, 2017, **12**(2), e0171558.
11 D. A. Nation, M. D. Sweeney, A. Montagne, A. P. Sagare, L. M. D'Orazio, M. Pachicano, F. Sepehrband, A. R. Nelson, D. P. Buennagel, M. G. Harrington, T. L. S. Benzinger, A. M. Fagan, J. M. Ringman, L. S. Schneider, J. C. Morris, H. C. Chui, M. Law, A. W. Toga and B. V. Zlokovic, Blood-brain barrier breakdown is an early biomarker of human cognitive dysfunction, *Nat. Med.*, 2019, **25**(2), 270–276.
12 A. Montagne, S. R. Barnes, M. D. Sweeney, M. R. Halliday, A. P. Sagare, Z. Zhao, A. W. Toga, R. E. Jacobs, C. Y. Liu, L. Amezcua, M. G. Harrington, H. C. Chui, M. Law and B. V. Zlokovic, Blood-brain barrier breakdown in the aging human hippocampus, *Neuron*, 2015, **85**(2), 296–302.
13 A. W. Tarudji, H. A. Miller, E. T. Curtis, C. L. Porter, G. L. Madsen and F. M. Kievit, Sex-based differences of antioxidant enzyme nanoparticle effects following traumatic brain injury, *J. Controlled Release*, 2023, **355**, 149–159.
14 B. A. Bony, H. A. Miller, A. W. Tarudji, C. C. Gee, A. Sarella, M. G. Nichols and F. M. Kievit, Ultrasmall Mixed Eu-Gd Oxide Nanoparticles for Multimodal Fluorescence and Magnetic Resonance Imaging of Passive Accumulation and Retention in TBI, *ACS Omega*, 2020, **5**(26), 16220–16227.
15 H. A. Miller, A. W. Magsam, A. W. Tarudji, S. Romanova, L. Weber, C. C. Gee, G. L. Madsen, T. K. Bronich and F. M. Kievit, Evaluating differential nanoparticle accumulation and retention kinetics in a mouse model of traumatic brain injury via K(trans) mapping with MRI, *Sci. Rep.*, 2019, **9**(1), 16099.
16 G. Stinnett, N. Taheri, J. Villanova, A. Bohloul, X. Guo, E. P. Esposito, Z. Xiao, D. Stueber, C. Avendano, P. Decuzzi, R. G. Pautler and V. L. Colvin, 2D Gadolinium Oxide Nanoplates as T(1) Magnetic Resonance Imaging Contrast Agents, *Adv. Healthcare Mater.*, 2021, **10**(11), e2001780.
17 S. Marangoni Valeria, O. Neumann, L. Henderson, C. Kaffes Caterina, H. Zhang, R. Zhang, S. Bishnoi, C. Ayala-Orozco, V. Zucolotto, A. Bankson James, P. Nordlander and J. Halas Naomi, Enhancing T1 magnetic resonance imaging contrast with internalized gadolinium(III) in a multilayer nanoparticle, *Proc. Natl. Acad. Sci.*, 2017, **114**(27), 6960–6965.
18 Z. Wang, F. Carniato, Y. Xie, Y. Huang, Y. Li, S. He, N. Zang, J. D. Rinehart, M. Botta and N. C. Gianneschi, High Relaxivity Gadolinium-Polydopamine Nanoparticles, *Small*, 2017, **13**(43), 1701830.
19 A. Priester, R. Waters, A. Abbott, K. Hilmas, K. Woelk, H. A. Millar, A. W. Tarudji, C. C. Gee, B. McDonald, F. M. Kievit and A. J. Convertine, Theranostic Copolymers Neutralize Reaction Oxygen Species and Lipid Peroxidation Products for the Combined Treatment of Traumatic Brain Injury, *Biomacromolecules*, 2022, **23**(4), 1703–1712.
20 D. A. Moore, L. Patterson and M. J. Miller, Selective Trialkylation of cyclen with tert-butyl bromoacetate, *Org. Synth.*, 2008, **85**, 10.
21 S. C. Deoni, T. M. Peters and B. K. Rutt, High-resolution T1 and T2 mapping of the brain in a clinically acceptable time with DESPOT1 and DESPOT2, *Magn. Reson. Med.*, 2005, **53**(1), 237–241.
22 S. C. Deoni, B. K. Rutt and T. M. Peters, Rapid combined T1 and T2 mapping using gradient recalled acquisition in the steady state, *Magn. Reson. Med.*, 2003, **49**(3), 515–526.
23 S. R. Barnes, T. S. Ng, A. Montagne, M. Law, B. V. Zlokovic and R. E. Jacobs, Optimal acquisition and modeling parameters for accurate assessment of low Ktrans blood-brain barrier permeability using dynamic contrast-enhanced MRI, *Magn. Reson. Med.*, 2016, **75**(5), 1967–1977.
24 A. K. Heye, M. J. Thrippleton, P. A. Armitage, M. D. C. Valdes Hernandez, S. D. Makin, A. Glatz, E. Sakka and J. M. Wardlaw, Tracer kinetic modelling for DCE-MRI quantification of subtle blood-brain barrier permeability, *Neuroimage*, 2016, **125**, 446–455.
25 M. Tripepi, F. Capuana, E. Gianolio, F. V. C. Kock, A. Pagoto, R. Stefania, G. Digilio and S. Aime, Synthesis of High Relaxivity Gadolinium AAZTA Tetramers as Building Blocks for Bioconjugation, *Bioconjugate Chem.*, 2018, **29**(4), 1428–1437.
26 M. Grogna, R. Cloots, A. Luxen, C. Jérôme, C. Passirani, N. Lautram, J.-F. Desreux and C. Detrembleur, Convenient grafting through approach for the preparation of stealth polymeric blood pool magnetic resonance imaging contrast agents, *J. Polym. Sci., Part A: Polym. Chem.*, 2011, **49**(17), 3700–3708.
27 P. Caravan, C. T. Farrar, L. Frullano and R. Uppal, Influence of molecular parameters and increasing magnetic field strength on relaxivity of gadolinium- and manganese-based T1 contrast agents, *Contrast Media Mol. Imaging*, 2009, **4**(2), 89–100.
28 L. Granato, S. Laurent, L. Vander Elst, K. Djanashvili, J. A. Peters and R. N. Muller, The Gd3+ complex of 1,4,7,10-tetraazacyclododecane-1,4,7,10-tetraacetic acid mono(p-

isothiocyanatoanilide) conjugated to inulin: a potential stable macromolecular contrast agent for MRI, *Contrast Media Mol. Imaging*, 2011, **6**(6), 482–491.

29 M. Ndiaye, V. Malytskyi, T. Vangijzegem, F. Sauvage, M. Wels, C. Cadiou, J. Moreau, C. Henoumont, S. Boutry, R. N. Muller, D. Harakat, S. D. Smedt, S. Laurent and F. Chuburu, Comparison of MRI Properties between Multimeric DOTAGA and DO3A Gadolinium-Dendron Conjugates, *Inorg. Chem.*, 2019, **58**(19), 12798–12808.

30 M. Rohrer, H. Bauer, J. Mintorovitch, M. Requardt and H.-J. Weinmann, Comparison of magnetic properties of MRI contrast media solutions at different magnetic field strengths, *Invest. Radiol.*, 2005, **40**(11), 715–724.

31 N. D. Donahue, H. Acar and S. Wilhelm, Concepts of nanoparticle cellular uptake, intracellular trafficking, and kinetics in nanomedicine, *Adv. Drug Delivery Rev.*, 2019, **143**, 68–96.

32 P. S. Tang, S. Sathiamoorthy, L. C. Lustig, R. Ponzielli, I. Inamoto, L. Z. Penn, J. A. Shin and W. C. Chan, The role of ligand density and size in mediating quantum dot nuclear transport, *Small*, 2014, **10**(20), 4182–4192.

33 C. Dalal and N. R. Jana, Multivalency Effect of TAT-Peptide-Functionalized Nanoparticle in Cellular Endocytosis and Subcellular Trafficking, *J. Phys. Chem. B*, 2017, **121**(14), 2942–2951.

34 V. N. Bharadwaj, C. Copeland, E. Mathew, J. Newbern, T. R. Anderson, J. Lifshitz, V. D. Kodibagkar and S. E. Stabenfeldt, Sex-Dependent Macromolecule and Nanoparticle Delivery in Experimental Brain Injury, *Tissue Eng., Part A*, 2020, **26**(13–14), 688–701.

35 R. Gupte, W. Brooks, R. Vukas, J. Pierce and J. Harris, Sex Differences in Traumatic Brain Injury: What We Know and What We Should Know, *J. Neurotrauma*, 2019, **36**(22), 3063–3091.